Journal of Wood Science

ORIGINAL ARTICLE

Open Access

An experimental and numerical study on the coupling effect of CLT wall-to-floor angle bracket connections

Xiaofeng Sun[1], Minjuan He[1*] and Zheng Li[1]

Abstract

Cross-laminated timber (CLT) wall panels are commonly connected to the floor or foundation using metal connections, which play a critical role in determining the seismic performance and energy dissipation of the CLT shear walls. In this study, to comprehend the tension–shear coupling effect of the CLT wall-to-floor angle bracket connections under seismic loads, both monotonic and cyclic shear tests were conducted on the angle brackets that were also simultaneously applied with different levels of prescribed vertical axial tension. The influence of the co-existent axial tension on the horizontal shear performance of the angle brackets was analyzed. Furthermore, a numerical model of the angle brackets was developed and validated with the experimental results, which could predict the tension–shear coupling effect based on the monotonic loading scenario. Based on the numerical model, parametric analysis was conducted, and an analytical tension–shear interaction diagram representing the coupling effect of the angle brackets under seismic loads was established. It is found that with an increase of the axial tension from 0 to 30 kN, the shear resisting capacity of the angle brackets is diminished by 33.29%, and the pinching effect of their hysteretic load–displacement curves is mitigated. When the number of the connection-to-floor screws of the angle brackets was increased from 10 to 14, the shear resisting capacity of the angle brackets can be enhanced by 6.43%, and their shear strength degradation can be relieved by 12.85–56.25%. For the CLT wall-to-floor angle brackets, the analytical interaction diagram can be described using one bilinear function, which consists of the ratio between the shear to the shear resistance and the ratio between the tension to the pull-out resistance.

Keywords Angle bracket, Tension–shear coupling effect, Seismic performance, Numerical model, Analytical interaction diagram

Introduction

Cross-laminated timber (CLT) is a massive engineered wood with the advantages of ideal integrity, large in-plane stiffness, excellent thermal insulation performance, etc. [1–3]. These advantages of CLT make it a competitive building material that is suitable for the floor diaphragms or the shear walls in mid- and high-rise timber structures. The CLT wall panels are commonly connected to the foundation or the floor diaphragms using hold-downs and angle brackets, forming one typical CLT shear wall structure. The hold-downs and the angle brackets are commonly connected to the floor diaphragms using screws or nails, or anchored to the foundation using bolts. The CLT wall panels can behave rigidly with an elastic behavior due to their high in-plane strength and stiffness. Therefore, the mechanical properties of the hold-downs or the angle brackets can almost dominate the seismic performance of the CLT shear wall structures [4–6].

*Correspondence:
Minjuan He
hemj@tongji.edu.cn
[1] Department of Structural Engineering, Tongji University, Shanghai 200092, People's Republic of China

During the early stage, most of the studies on CLT focus on comprehending the mechanical properties of typical CLT connections (e.g., hold-downs, angle brackets, etc.), which serves as a basis for the subsequent studies on CLT shear walls. Gavric et al. [7] conducted hysteretic tests on hold-downs and angle brackets, and the cyclic loading was applied along the vertical tension direction and the horizontal shear direction separately. It is found that the two typical CLT connections can provide desirable ductility and good energy dissipation. Tomasi and Smith [8] tested the shear performance of the specially designed wall-to-foundation angle brackets. It was emphasized that experiment-based studies were the only reliable means of determining the design capacities of the connections. Hossain et al. [9] investigated the feasibility of using self-tapping screw assemblies with a double inclination of fasteners for the shear connection of CLT panels. The connection assembly with a double inclination of fasteners can provide excellent structural performance and the required ductility for the system. Izzi et al. [10] conducted vertical tension tests on CLT steel-to-timber joints fastened by annular-ringed shank nails. The experimental tensile capacity was consistent with the predictive one based on the provisions from the European Technical Assessment (ETA) [11]. Sun et al. [12] analyzed the seismic performance of the CLT shear wall structures equipped with the *U*-shaped flexural plate (UFP) connections as the dissipaters. It was approved that the UFP connections could effectively reduce the absolute horizontal accelerations of the structures under seismic loads. Overall, it is deemed that the CLT connections can provide substantial resistance in orthogonal directions (i.e., the vertical and the horizontal directions), and their ductility can affect the energy-dissipating capacities of the CLT structures. For simplification, the aforementioned studies were conducted based on a design assumption that the rocking mechanism and the slip mechanism of the shear walls act independently. Therefore, the shear behavior and the tensile behavior of the connections were considered uncoupled in these studies.

For one multi-story CLT shear wall structure under the seismic loads, the rocking and the slip mechanisms of its shear walls actually act jointly on the wall-to-floor and the wall-to-foundation connections. A series of studies have focused on the tension–shear coupling effect of the CLT connections, which can be described as a phenomenon that the vertical tension behavior (i.e., axial tension behavior) of the connections can affect their horizontal shear behavior and vice versa. Liu and Lam [13, 14] conducted a series of tests with a specially designed setup to investigate the coupling effect of both CLT hold-downs and angle brackets. It was found that the co-existent axial tension could significantly reduce the shear resistance of the hold-downs or the angle brackets. Subsequently, Liu et al. [15] modeled the coupling effect of hold-downs using a finite element-based algorithm called HYST, which was originally used for simulating the mechanical behavior of nail-based timber connections. In Liu's studies [13–15], the tested angle brackets and hold-downs were designed to connect the CLT shear walls to the steel foundation. Pozza et al. [16] tested the tension–shear coupling effect of the CLT wall-to-foundation hold-downs. It was found that the axial mechanical properties of the hold-downs could be affected by the lateral deformation imposed on the hold-downs. Then, Pozza et al. [17] developed a novel coupled tension–shear numerical model capable of predicting the coupling response of the hold-downs under general loading scenarios.

Commenting on the tension–shear interaction relationship of CLT connections in a quantitative manner has become one critical task, which can facilitate a safer seismic design of CLT connections. Izzi et al. [18] developed a novel finite element model of the wall-to-floor angle bracket or hold-down, which was bolted to the floor diaphragm. In that model, by varying the inclination of the load representing the simultaneously applied lateral and axial loads, based on numerical analysis, an analytical quadratic tension–shear interaction relationship was obtained for the CLT connections. D'Arenzo et al. [19, 20] conducted monotonic tests on novel CLT wall-to-floor angle brackets in tension and shear directions separately. A quadratic tension–shear interaction was recommended for the angle brackets based on numerical analysis. The work conducted by D'Arenzo for deriving the interaction relationship was similar to that conducted by Izzi et al. [18]. By assuming a quadratic tension–shear coupling effect, Masroor et al. [21] investigated the influence of the bi-axial contribution of the angle brackets on the lateral performance of the CLT shear walls. In the model, the lateral displacements and the rotations of the walls were decreased once considering the coupling effect of the connections, which indicated the necessity of considering the tension–shear coupling effect in engineering design.

Based on the aforementioned literature review, it is found that the analytical tension–shear interaction relationship in some studies was obtained mainly based on the connection tests with a loading scenario of axial tension or horizontal shear separately rather than based on tests with simultaneously applied tension and shear. Furthermore, experimental studies on the coupling effect of the wall-to-floor angle brackets fastened with self-tapping screws are limited. To explicitly address the issues, monotonic and cyclic shear tests were conducted on CLT wall-to-floor angle brackets, which were simultaneously applied with different levels of prescribed axial tension. The tension–shear coupling effect of the angle brackets under seismic loads was studied, and their horizontal shear performance was analyzed with respect to different levels of co-existent axial tension. Subsequently, a numerical model of the wall-to-floor angle brackets was developed and validated. Based on the parametric analysis, an analytical tension–shear interaction diagram representing the coupling effect of the angle brackets under seismic loads was established. The results can deepen the comprehension of the coupling effect of CLT connections under seismic loads, resulting in a more rational and efficient seismic design procedure for CLT connections.

Experimental program

In this study, the CLT wall-to-floor angle brackets were tested with the axial tension and the horizontal shear applied simultaneously. The loading setup was specially designed to minimize the influence of the eccentricity effect of the axial tension on the horizontal cyclic shear tests of the angle brackets. The test setup, the specimen details, and the loading protocol are introduced in this section.

Test setup

The test setup was specially designed to implement the bi-axial monotonic and cyclic loading tests on CLT angle brackets, as shown in Fig. 1. The assembly of the CLT panels connected by the two angle brackets was deemed as the specimen in the study. A 1.7-m-length steel cable with a 15.2-mm diameter was used to vertically connect the specimen and the steel load-transfer frame for applying the prescribed axial tension, as shown in Fig. 1b. The maximum lateral displacement of the specimen imposed by the actuator was around 80 mm. Therefore, during the test, the angle between the steel cable and the vertical direction was 3 degree at most, which could minimize the influence of the eccentric tension on the horizontal monotonic or cyclic shear tests. The steel load-transfer frame was jacked up and the jack was connected in series with a load cell below. The load cell was supported by a steel beam. The load-transfer frame can transfer the force provided by the jack to the steel cable, which is finally applied on the specimen. Therefore, during the test, the axial force applied on the specimen can be measured by the load cell in series with the jack.

The horizontal shear test was implemented using the actuator, which could apply cyclic and monotonic shear forces close to the bottom of the CLT wall panel to minimize the induced turning moment. The horizontal shear was actually applied to the centroid of the screws that connect the vertical leg of the angle bracket to the wall, and was then transferred through the angle bracket to the CLT floor below, as shown in Fig. 1b. A pair of wall-to-floor angle brackets were included per specimen. They were located, respectively, on the front side and the rear side of the wall panel, forming a symmetrical testing system. The HBS self-tapping screws with a dimension of 5 mm × 80 mm (diameter × length) were used to connect the angle brackets to the floor diaphragm and the wall panel. A pair of "L" shaped steel shear keys was mounted on the steel foundation to restrict the horizontal movement of the specimen, as shown in Fig. 1b. In the specimen, one gap with a width equal to the wall thickness was arranged between the neighboring CLT floor diaphragms. The gap between the floor diaphragms was also located below the wall panel, as shown in Fig. 1c. As a result, the CLT wall panel did not contact the CLT floor diaphragms, which could eliminate the CLT wall-to-floor friction. In this study, the relative horizontal displacement between the CLT wall and the CLT floor diaphragms was measured using linear voltage displacement transducers (LVDTs). The relative displacement measured by the LVDTs was adopted as the shear deformation of the angle bracket under the horizontal shear force, considering that no significant rocking movement was observed for the CLT wall panel during the tests.

Specimen details

The plane size of the CLT wall panel and that of the CLT floor diaphragms were 300 mm × 450 mm and 300 mm × 300 mm, respectively. These five-layer non-edge-glued CLT panels were fabricated with the No. 2 grade spruce-pine-fir (SPF) lumber [22] with a cross-sectional area of 140 mm × 35 mm (width × thickness). Therefore, the thickness of the 5-layer CLT panels was 175 mm. The average moisture of the CLT panels was 12.1% with a coefficient of variation (COV) of 9.5%, and all the tests were conducted in an indoor environment with a relative humidity (RH) of 50% and an average temperature of 25 Celsius. The spacing from the center of the two angle brackets per specimen to the lateral side of the CLT wall or floor panel was equal to half of the CLT width, which was 150 mm.

The tested wall-to-floor angle brackets were welded using 5-mm-thickness Q235 steel plates. The configurations of the angle brackets are shown in Fig. 2. The angle bracket was designed by the authors, which represented the type of the connections commonly used in CLT construction. It was attested that the angle bracket could provide desirable hysteretic performance along the horizontal shear direction based on the tests conducted by Sun et al. [23]. In this study, the angle brackets of the specimens can be divided into the normal group and the strengthening group. In the normal group, the angle brackets of the specimens were partial-screwing;

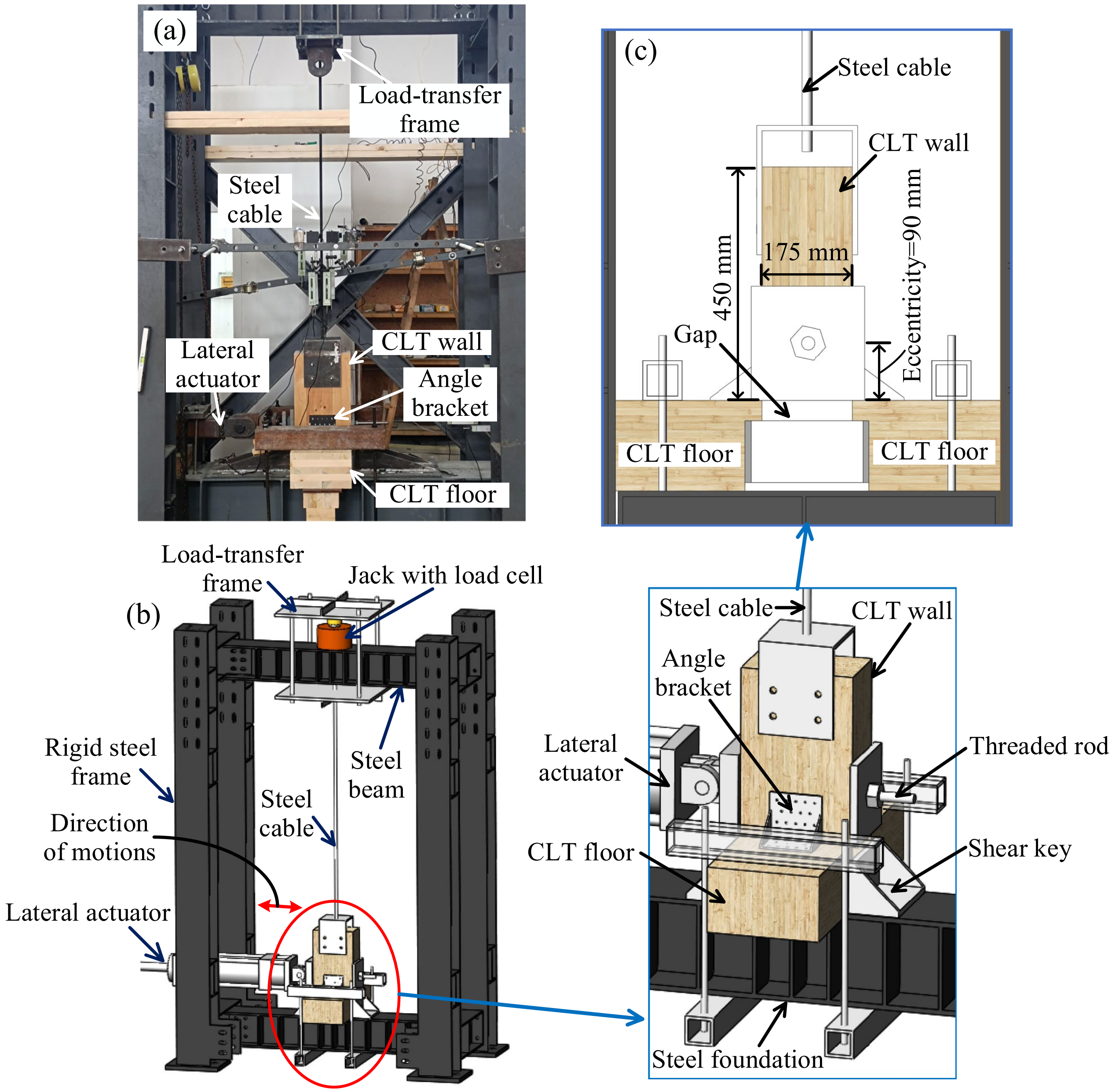

Fig. 1 Test setup: **a** global view; **b** geometrical details; **c** side view

by contrast, in the strengthening group, the angle brackets of the specimens were fully screwing, as illustrated in Fig. 2. In both the normal group and the strengthening group, the vertical legs of the angle brackets were connected to the CLT wall using eight 5 mm × 80 mm self-tapping screws (Fig. 2b). Furthermore, for the angle brackets in the normal group and those in the strengthening group, ten 5 mm × 80 mm self-tapping screws and fourteen 5 mm × 80 mm self-tapping screws were used to connect their horizontal legs to the CLT floor, respectively (Fig. 2c). All the screws were fully threaded, which were provided by the manufacturer of Rothoblaas from Italy.

Loading protocol

For reproducing the tension–shear coupling loading scenario, a constant prescribed vertical tension was applied and maintained to the specimen containing a pair of angle brackets. Subsequently, along the horizontal direction, monotonic and cyclic shear tests were implemented on the specimen to investigate the coupling effect of the included angle brackets based on a

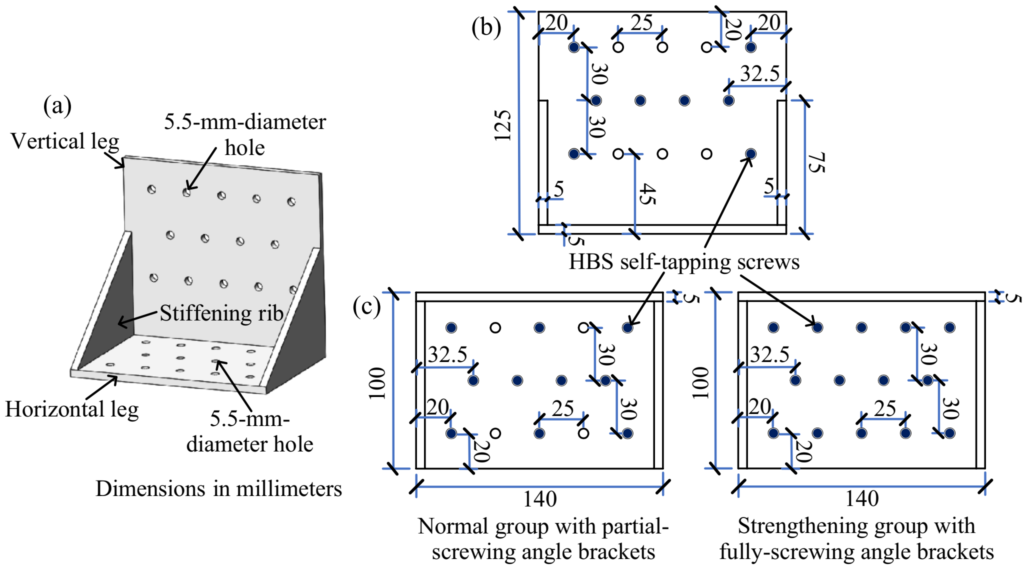

Fig. 2 Angle bracket connection: **a** global view; **b** front view; **c** top view

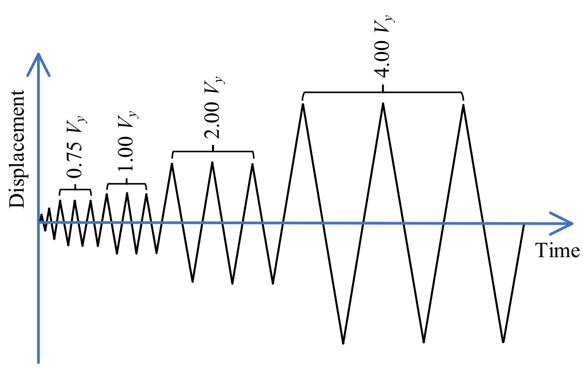

Fig. 3 The loading protocol for the cyclic shear tests [24]

displacement-based loading protocol from EN 12512 [24]. A loading rate of 0.2 mm/s and that of 0.8 mm/s were adopted in the monotonic shear tests and in the cyclic shear tests, respectively. The loading protocol for the cyclic shear tests is shown in Fig. 3. The specimens were loaded until the included angle brackets were damaged. V_y represents the yielding displacement of the angle brackets obtained from the monotonic shear tests, which varied from configuration to configuration. Such a tension–shear coupling loading scenario might be different from that actually applied to one angle bracket mounted in CLT shear walls, which was subjected to simultaneous variations in both tension and shear [25]. Whereas the adopted loading scenario can allow to obtain: (1) the influence of the axial tension on the shear behavior of the angle brackets; (2) an analytical interaction diagram representing the tension–shear coupling relationship of the angle brackets.

The hysteretic shear tests and the pull-out tests were conducted on the 5 mm × 80 mm self-tapping screws to obtain their shear strength and pull-out strength, respectively. The hysteretic shear tests were conducted on totally 10 self-tapping screws. The loading protocol of the hysteretic shear tests was defined based on EN 12512 [24], and the loading rate was adopted as 6 mm/min. The pull-out tests were conducted on totally 10 self-tapping screws, and the loading rate was adopted as 1 mm/min. Based on these tests on the self-tapping screws, the characteristic shear strength along the CLT major strength direction and the characteristic pull-out strength were obtained as 4.03 kN and 2.87 kN, respectively. Besides, based on the coupon tests on the steel used for the angle brackets, the design yield strength was obtained as 280 MPa. The axial tensile resistance of the two angle brackets per specimen should be the minimum value of the total pull-out resistance and the total shear resistance of the self-tapping screws. It was estimated as 57.4 kN and 64.5 kN for the specimen in the normal group and that in the strengthening group, respectively. A strength safety factor of 2.5 should be considered when determining the design strength of the connections [26]. Therefore, four different levels of constant axial tension T that applied on the specimens were adopted in the tests, which were 0 kN, 10 kN, 20 kN, and 30 kN. In this study, one monotonic shear test and three cyclic shear tests were conducted on the specimen, which was simultaneously applied with one prescribed constant tension. Besides, when the applied axial tension T was 30 kN, both the specimens of the normal group and those of the strengthening group were tested under the monotonic and cyclic shear loadings. The test matrix is listed in Table 1.

Experimental results

The damage modes and load–displacement curves are presented for the 5 specimens under the monotonic shear loading scenario and 15 specimens under the cyclic shear loading scenario. Besides, the key mechanical characteristics of the angle brackets (i.e., secant stiffness, shear strength degradation, and energy dissipation) are presented in this section.

Damage modes

An eccentricity of 90 mm inevitably existed from the horizontal shear forces to the bottom of the CLT wall panel, as shown in Fig. 1c. Therefore, during the loading procedure of the horizontal cyclic shear, with an increase of the shear force, the induced turning moment applied on the CLT wall was enhanced. When no axial tension was applied on the specimens (i.e., T0C1–T0C3), little deformation could be observed in the connection-to-wall screws during the early stage of the loading procedure. Whereas, during the end of the loading procedure, significant rotational tendency relative to the angle bracket was observed in the CLT wall panel, as shown in Fig. 4a. It resulted in the shear breakages of the connection-to-wall screws that located close to the corner of the angle bracket. Furthermore, the eccentricity from the centroid of the eight screws drilled in the vertical leg to the surface of the floor would cause a slight overturning moment to

Table 1 Test matrix

No.	Tension *T* (kN)	Type	Monotonic	Cyclic
1	0	Normal group	T0M1	T0C1, T0C2, T0C3
2	10	Normal group	T10M1	T10C1, T10C2, T10C3
3	20	Normal group	T20M1	T20C1, T20C2, T20C3
4	30	Normal group	T30M1	T30C1, T30C2, T30C3
5		Strengthening group	ST30M1	ST30C1, ST30C2, ST30C3

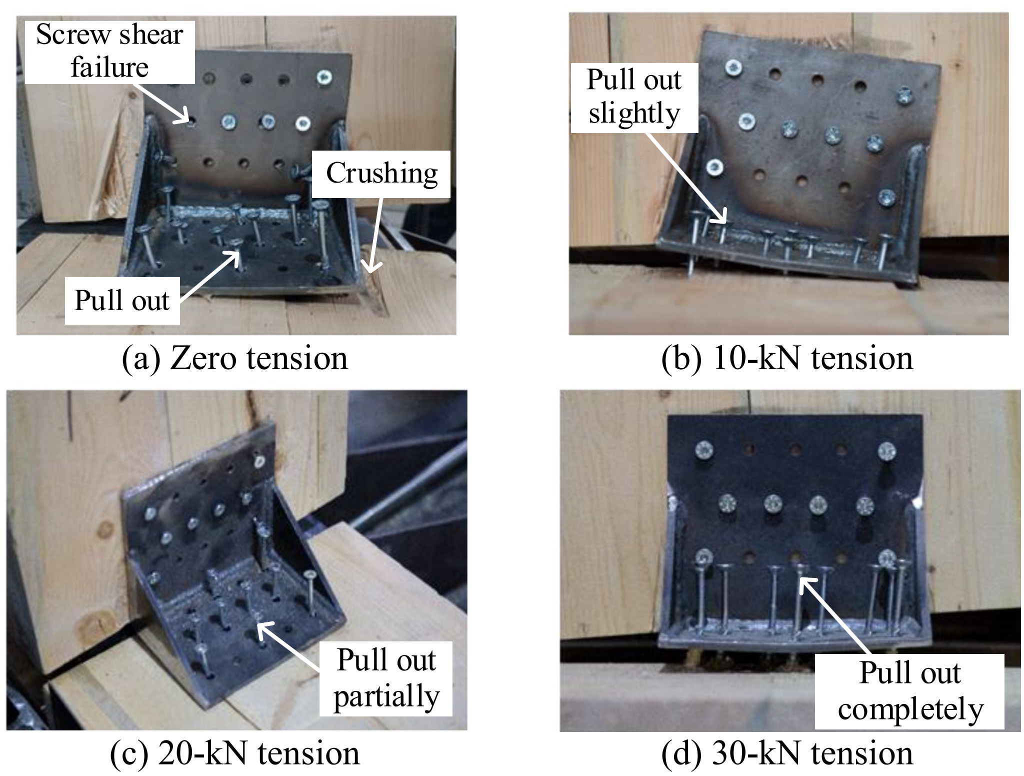

Fig. 4 Damage modes of the specimens in the normal group

be applied on the angle bracket. The overturning moment was coupled with the horizontal shear applied by the actuator. During the loading procedure, the angle bracket was rotationally deformed by the overturning moment. Therefore, when no axial tension was applied on the specimens (i.e., T0C1–T0C3), the connection-to-floor screws of the angle brackets were pulled out, as shown in Fig. 4a. Due to the reinforcement of the stiffening ribs, little stretch deformation was observed at the "L" corner of the angle brackets. After the tests, slight flexural deformation could be identified on the horizontal legs of the angle brackets. Besides, by providing bearing due to contact, the CLT floor could restrain the rotation movement of the angle brackets caused by the induced overturning moment. Therefore, localized crushing occurred on the CLT floor diaphragm.

When axial tension was applied and maintained to the specimens (i.e., T10C1–T10C3, T20C1–T20C3, T30C1–T30C3), no shear breakages occurred on the connection-to-wall screws. It is because when a constant axial tension was applied on the specimens, the induced turning moment applied on the CLT wall panels was reduced due to the decrease in lever arm. A larger axial tension could result in a more severe pull-out of the connection-to-floor screws after the cyclic shear loading. Besides, in the normal group, when the axial tension was 30 kN, a complete pull-out of the screws was observed in the angle brackets, as shown in Fig. 4d. It is noticed that the localized crushing of the CLT floor could be mitigated by enhancing the axial tension. It is because during the tests, an enhanced axial tension would enlarge the gap between the angle brackets and CLT floor, which could relieve the bearing on the angle brackets due to contact provided by the CLT floor. For an identical axial tension, compared to the monotonic shear loading scenario, the cyclic shear loading scenario could cause a more severe pull-out of the screws. It is because the cyclic shear loading scenario could broaden the preliminary gap between the screws and the surrounding CLT more efficiently. Therefore, the CLT embedment stress applied on the screws was declined, resulting in a more significant degradation of the pull-out resistance of the self-tapping screws.

When the axial tension was 30 kN, for the angle brackets of the specimens in the normal group (i.e., T30C1–T30C3), a complete pull-out of the 10 connection-to-floor screws was observed under the cyclic shear loading. Therefore, for the angle brackets of the specimens in the strengthening group, totally 14 connection-to-floor screws were used to connect them to the floor diaphragm for the purpose of strengthening. When the co-existent axial tension was 30 kN, cyclic shear tests were conducted on the angle brackets of the specimens in the strengthening group (i.e., ST30C1–ST30C3). Their damage modes are shown in Fig. 5. For the specimens labeled as ST30C1 and ST30C3, the included angle brackets were damaged with shear breakages of their connection-to-wall screws combined with significant plastic deformation (Fig. 5a). Besides, for the specimen labeled as ST30C2, the included angle brackets were damaged with tearing and even de-lamination failure of the CLT floor laminas (Fig. 5b). After the tests, little flexural deformation could be identified on the horizontal legs of the angle brackets included in the three specimens of the strengthening group. It is because during the coupling tests, the horizontal legs of the angle brackets were tightly attached to the upper surface of the CLT floor. Therefore, almost no gap existed along the interface between the horizontal leg and the CLT floor, which

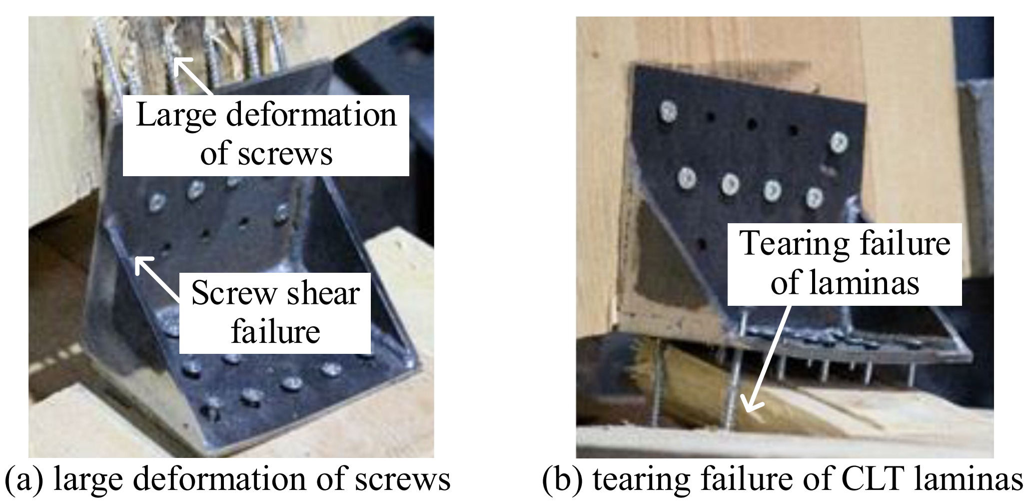

Fig. 5 Damage modes of the specimens in the strengthening group

resulted in a relatively uniform distribution of bearing due to contact provided by the floor.

Load–displacement curves

The load–displacement curves of the angle brackets under monotonic shear loading are shown in Fig. 6. The *X*-axis value represents the relative displacement measured by the LVDTs, which is approximated as the shear deformation of the angle bracket. The performance parameters of the angle brackets under monotonic shear loading are listed in Table 2. It shows that the initial shear stiffness k_{el} (i.e., the force-to-displacement ratio of the elastic phase) is almost identical despite the co-existent axial tension varies. The k_{el} of the angle brackets is around 2.750 kN/mm. For the angle brackets of the specimens in the normal group, with an increase of the axial tension T, their shear resisting capacity $F_{v,max}$ declines. Therefore, the ratio between the T and the $F_{v,max}$ enhances significantly with an increase of the T, as listed in Table 2. The $F_{v,max}$ of the angle brackets of the specimen T30M1 under a 30-kN tension is reduced to 48.37 kN. Whereas, when strengthening these angle brackets using 14 screws to connect their horizontal legs to the floor diaphragms (i.e., ST30M1), the $F_{v,max}$ increases by 23.2%. Based on the method "b" provided by EN 12512 [24] for defining the elastic and the post-elastic properties, the yielding displacement V_y was obtained as 20.05 mm, 12.02 mm, 10.49 mm, 10.61 mm, and 10.67 mm, for the specimens labeled as T0M1, T10M1, T20M1, T30M1, and ST30M1, respectively. Then, the loading protocol for the cyclic shear tests could be determined. Based on the specially designed coupling test setup, the entire procedure of the coupling tests is introduced as follows: (1) the axial tension at a target level was preliminarily applied to the specimen within 5 s, which was maintained at this level approximately during the following cyclic shear loading procedure by controlling the jack; (2) the cyclic shear loading protocol was applied to the specimen until significant damages occurred or the shear force dropped to 80% of the $F_{v,max}$. Load–displacement curves of the angle brackets per specimen in the strengthening group and those of the angle brackets per specimen in the normal group are shown in Figs. 7 and 8, respectively.

A slight oscillation around the target value existed in the co-existent axial tension, which was recorded by the load cell during the cyclic shear loading procedure (Fig. 9). It was due to the influence of the cyclic

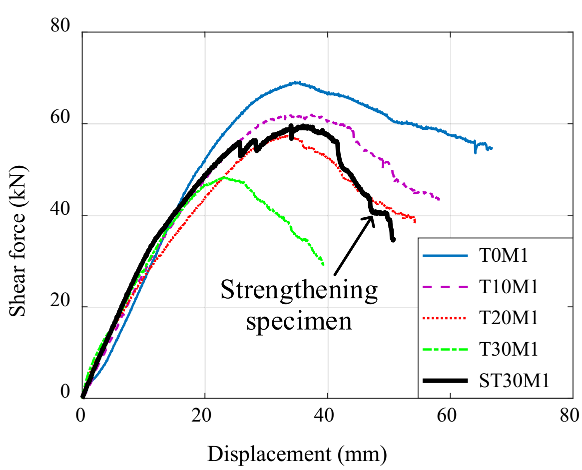

Fig. 6 Monotonic load–displacement curves of all the specimens

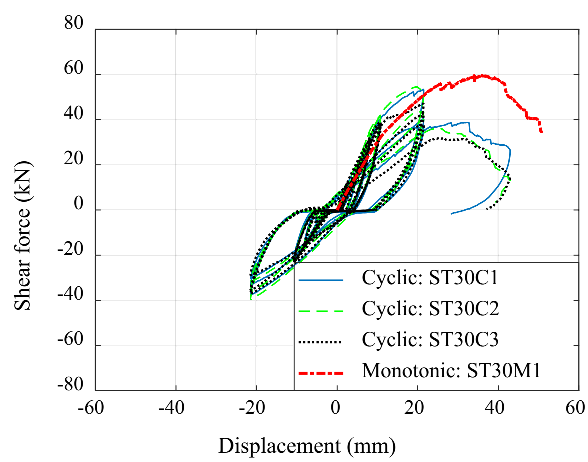

Fig. 7 Load–displacement curves of the specimens in the strengthening group

Table 2 Performance parameters of the angle brackets under monotonic shear loading

ID	T (kN)	$F_{v,max}$ (kN)	$T/F_{v,max}$	$F_{v,y}$ (kN)	V_y (mm)	k_{el} (kN/mm)	Average k_{el} (kN/mm)
T0M1	0	69.15	0	52.25	20.05	2.629	2.750
T10M1	10	62.05	0.161	32.30	12.02	2.710	
T20M1	20	57.43	0.348	27.17	10.49	2.612	
T30M1	30	48.37	0.620	29.34	10.61	2.789	
ST30M1	30	59.59	0.503	31.84	10.67	3.010	

$F_{v,y}$ represents the yielding shear force

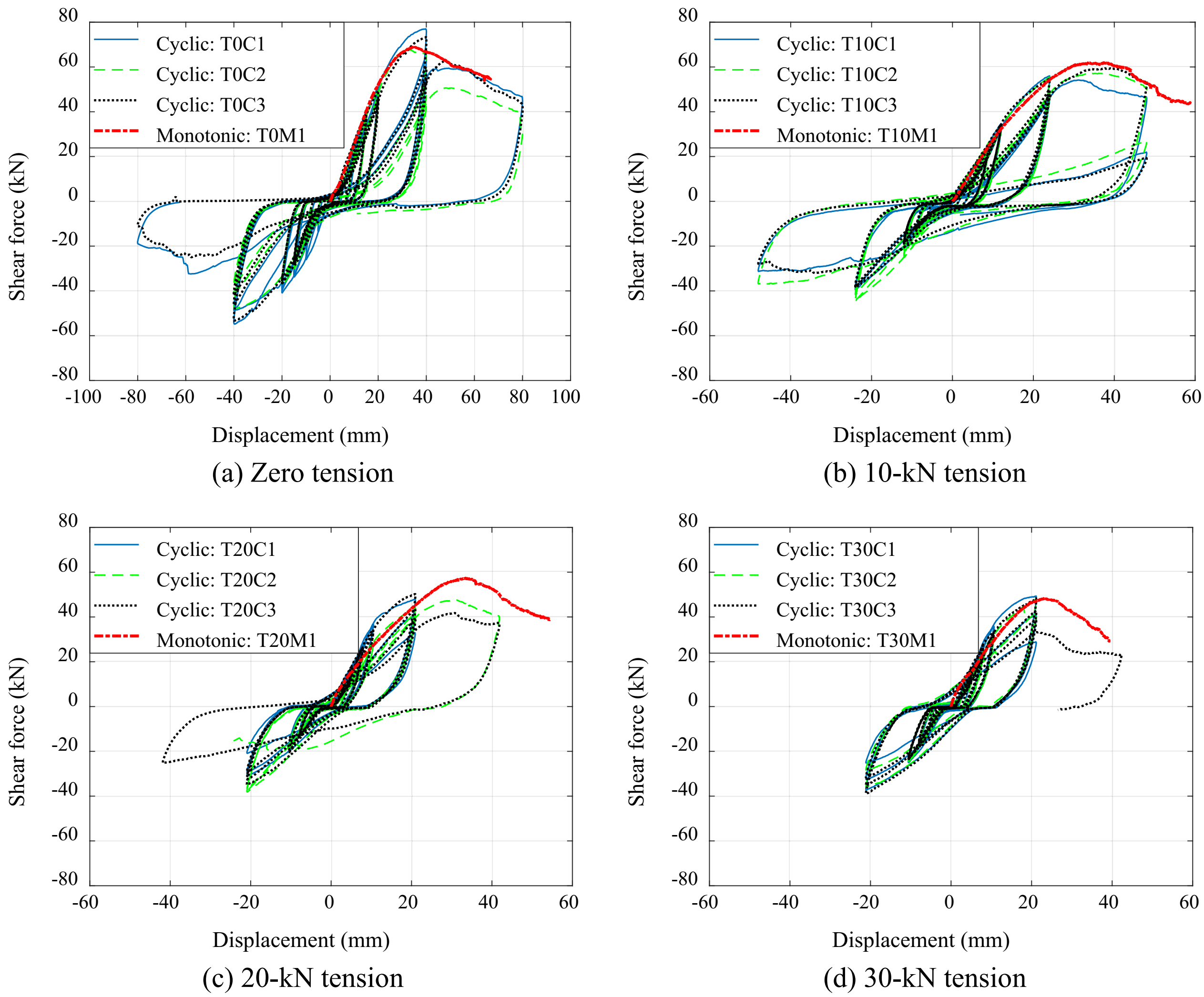

Fig. 8 Load–displacement curves of the specimens in the normal group

movement of the wall panel along the horizontal direction during the tests. The shear-resisting capacity of the two angle brackets per specimen is listed in Table 3. For the specimens of T20C1, T30C1, and T30C2, the included angle brackets carried less cycles of shear loading. When finishing the second or the third cycle with the amplitude of $2V_y$, premature pull-out failure occurred on the connection-to-floor screws of the angle brackets in these specimens. It indicates that the angle brackets are more prone to the pull-out failure with an increase of the T applied on the angle brackets, resulting in a higher ratio between T to $F_{v,max}$ (See Table 3). By contrast, the angle brackets in other specimens were tested under a cyclic shear loading until the first or the second circle with the amplitude of $4V_y$ was finished, as listed in Table 3. For the specimens of T20C1, T30C1, and T30C2, the $F_{v,max}$ of the included angle brackets carrying less cycles of shear loading is much close to that of the angle brackets in the specimens that has experienced a cycle with the amplitude of $4V_y$. It means the premature pull-out failure occurring in the connection-to-floor screws of the angle brackets does not significantly weaken the shear resistance of the angle brackets. It is because for the specimens of T20C1, T30C1, and T30C2, the $F_{v,max}$ of the included angle brackets has already been reached within the cycles with the amplitude of $2V_y$.

Overall, with an increase of the co-existent axial tension T from 0 to 30 kN, the average $F_{v,max}$ of the specimens in the normal group is diminished from 72.75 to 48.53 kN. It should be noted that for the angle brackets of the specimens under cyclic shear loading, their $F_{v,max}$ declines significantly with an increase of the axial tension T from 0 to 10 kN, and then to 20 kN. Whereas, when further enhancing the axial tension T from 20

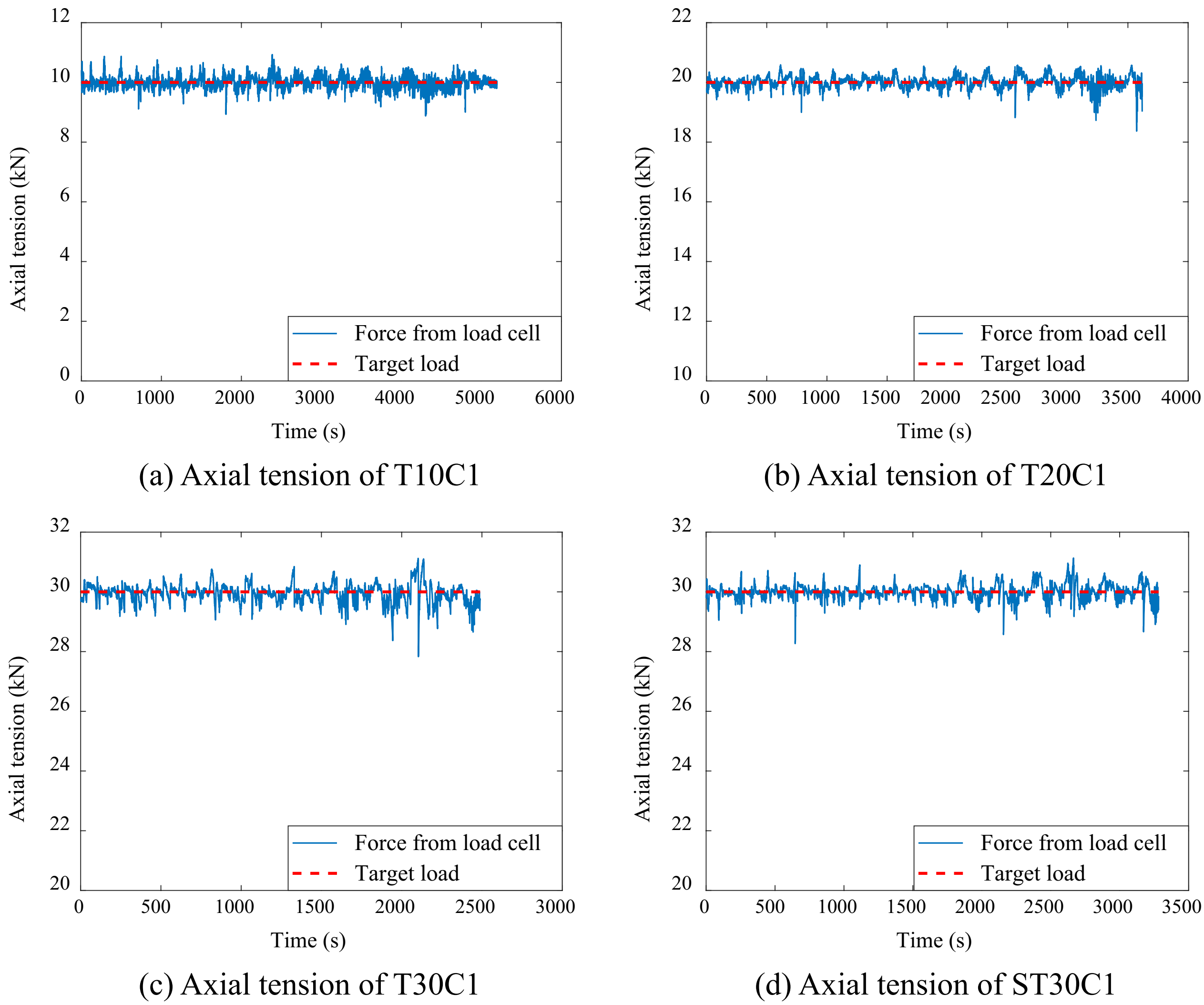

Fig. 9 The axial tension applied on the specimens during the cyclic shear tests

to 30 kN, the $F_{v,max}$ is almost unchanged. It is because for the angle brackets included in the specimen under a 20-kN axial tension, their connection-to-floor screws had been pulled out partially (Fig. 4c) within the cycles with the amplitude of $2V_y$. It hindered the further enhancement of the shear force of the angle brackets when subjected to the following cyclic shear loading. Besides, for the angle brackets of the specimens under a 30-kN axial tension, preliminary pull-out failure still occurred in their connection-to-floor screws within the cycles with the amplitude of $2V_y$. When the preliminary pull-out failure occurred, the shear deformation of the angle brackets under a 30-kN axial tension was much close to that of the angle brackets under a 20-kN axial tension (i.e., around 18 mm). Therefore, when enhancing the axial tension T from 20 to 30 kN, the $F_{v,max}$ is almost undiminished.

Compared to the angle brackets in the specimens of T30C1–T30C3, for the angle brackets in the specimens of ST30C1–ST30C3, their preliminary pull-out failure was postponed due to the strengthening using more connection-to-floor screws. When the preliminary pull-out failure occurred, the corresponding shear deformation of the angle brackets in the specimens of ST30C1–ST30C3 was larger. When under a co-existent axial tension T of 30 kN, the average $F_{v,max}$ of the specimens in the strengthening group is 6.43% higher than that of the specimens in the normal group, as listed in Table 3. Namely, when strengthening the angle brackets using additional four self-tapping screws to connect their horizontal legs to the CLT floor, their average $F_{v,max}$ can be enhanced from 48.53 to 51.65 kN. Actually, the $F_{v,max}$ of the ST30C1 is 11.9% less than that of the ST30C2 and 13.5% less than that of the ST30C3, respectively. It is caused by the

Table 3 Shear resisting capacity of the tested angle brackets

Group	Tension *T* (kN)	ID	$F_{v,max}$ (kN)	$T/F_{v,max}$	Final cycle	Average $F_{v,max}$
Normal	0	T0C1	67.83	0	1st cyclic of the amplitude of $4V_y$	72.75 kN (COV = 6.3%)
		T0C2	73.53	0	1st cyclic of the amplitude of $4V_y$	
		T0C3	76.89	0	1st cyclic of the amplitude of $4V_y$	
	10	T10C1	56.02	0.178	2nd cyclic of the amplitude of $4V_y$	57.44 kN (COV = 2.8%)
		T10C2	57.13	0.175	2nd cyclic of the amplitude of $4V_y$	
		T10C3	59.18	0.169	2nd cyclic of the amplitude of $4V_y$	
	20	T20C1	47.27	0.423	3rd cyclic of the amplitude of $2V_y$	48.54 kN (COV = 3.3%)
		T20C2	47.98	0.417	1st cyclic of the amplitude of $4V_y$	
		T20C3	50.37	0.397	1st cyclic of the amplitude of $4V_y$	
	30	T30C1	47.81	0.627	2nd cyclic of the amplitude of $2V_y$	48.53 kN (COV = 1.6%)
		T30C2	48.42	0.620	3rd cyclic of the amplitude of $2V_y$	
		T30C3	49.37	0.608	1st cyclic of the amplitude of $4V_y$	
Strengthening	30	ST30C1	47.07	0.637	1st cyclic of the amplitude of $4V_y$	51.65 kN (COV = 7.7%)
		ST30C2	53.43	0.561	1st cyclic of the amplitude of $4V_y$	
		ST30C3	54.44	0.551	1st cyclic of the amplitude of $4V_y$	

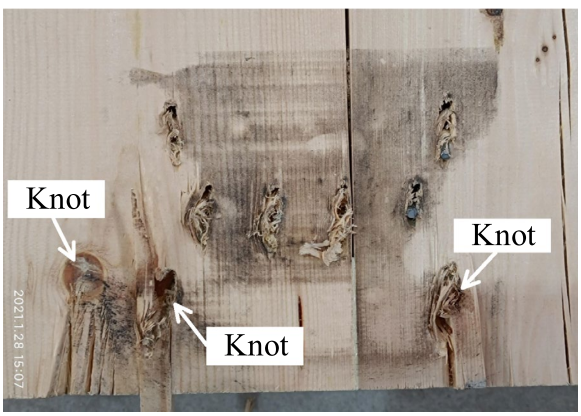

Fig. 10 Knots existing in the connection area from the CLT wall panel

wood defect (i.e., the knots) existing in the connection area from the CLT wall panel, as shown in Fig. 10. For the specimens of ST30C2–ST30C3, their average $F_{v,max}$ is 11.1% higher than that of the specimens in the normal group. Since the $F_{v,max}$ of the ST30C1 is significantly less than that of the ST30C2 or ST30C3, the COV for the specimens of ST30C1–ST30C3 is higher than that for the specimens of T30C1–T30C3. Furthermore, a significant pinching effect can be observed in the load–displacement curves of the angle brackets in the specimens under the 0-kN axial tension, as shown in Fig. 8a, and a similar conclusion was also stated by Gavric et al. [7, 27]. Whereas, with an increase of the axial tension *T*, the pinching effect is mitigated, as reflected by the hysteretic curves in Fig. 8b–d. It is because during the cyclic shear loading, the gap between the screws and the surrounding CLT laminas could be eliminated due to the co-existent axial tension. A similar conclusion was also stated by Liu et al. [13].

Mechanical characteristics

Secant stiffness

The secant stiffness K_i was calculated for the cycle *i* of the experimental load–displacement curves using the Eq. (1), in which, F_i represents the maximum shear force of cycle *i*; Δ_i represents the displacement corresponding to the F_i. The curves of the calculated secant stiffness for the angle brackets of the specimens in the normal group and those for the angle brackets of the specimens in the strengthening group are shown in Figs. 11 and 12, respectively. Besides, for the angle brackets in the specimens of C1–C3, their average K_i corresponding to the cycles with an identical amplitude was calculated, which was marked below the secant stiffness curves. It is found that the secant stiffness of the first or the second cycle (i.e., K_1 or K_2) is smaller than that of the following cycles. It is because when during the cycles of 1–2 with an amplitude less than $0.50V_y$, just embedment deformation occurred in the CLT subjected to the compression from the inserted screws, and almost no elastic deformation existed in the screws. By contrast, when during the cycles of 3–8 with an amplitude ranging from $0.50V_y$ to $0.75V_y$, significant elastic deformation occurred in the screws besides the embedment deformation occurring in the CLT due to the compression from the screws. Therefore, the secant stiffness of the cycles of 1–2 is smaller than that of the cycles of 3–8. For the cycles of 3–5 with an amplitude of $0.75V_y$ and for the cycles of 6–8 with an amplitude of $1.0V_y$, their corresponding secant stiffness remains stable, which indicates that the angle brackets

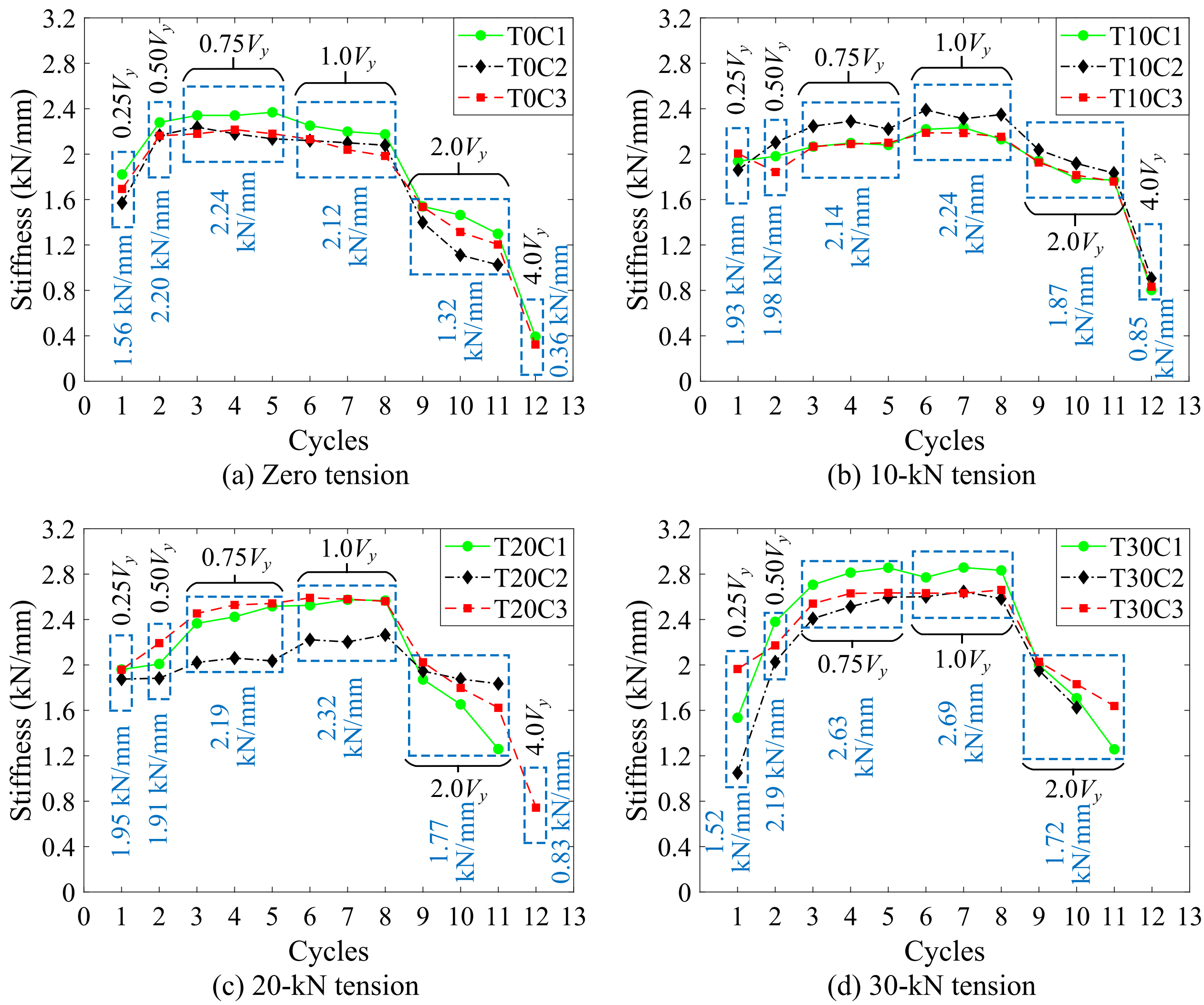

Fig. 11 Scant stiffness of the angle brackets in the specimens of the normal group

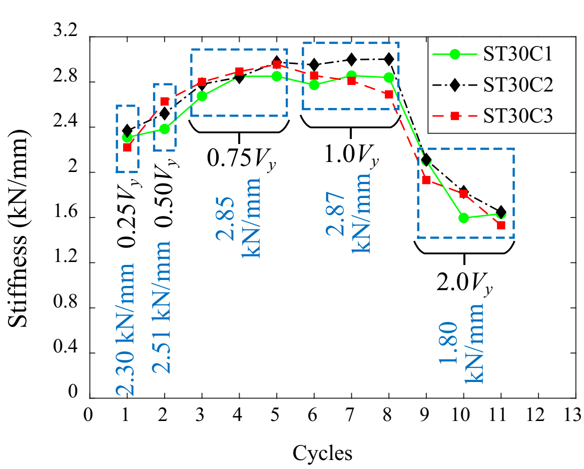

Fig. 12 Scant stiffness of the angle brackets in the specimens of the strengthening group

are within the elastic phase. When the angle brackets were loaded to the cycles with an amplitude of $2.0V_y$ or more, damages occurred in the angle brackets with plastic deformation existing in their screws, resulting in the degradation of the secant stiffness, as shown in Figs. 11 and 12.

$$K_i = \frac{|+F_i| + |-F_i|}{|+\Delta_i| + |-\Delta_i|} \tag{1}$$

Since the secant stiffness of the cycles with the amplitudes of both $0.75V_y$ and $1.0V_y$ is relatively stable, the secant stiffness corresponding to the amplitude of $0.75V_y$ or $1.0V_y$ is compared with respect to different levels of the co-existent axial tension, as shown in Fig. 13. With an increase of the axial load, a growing trend of the secant

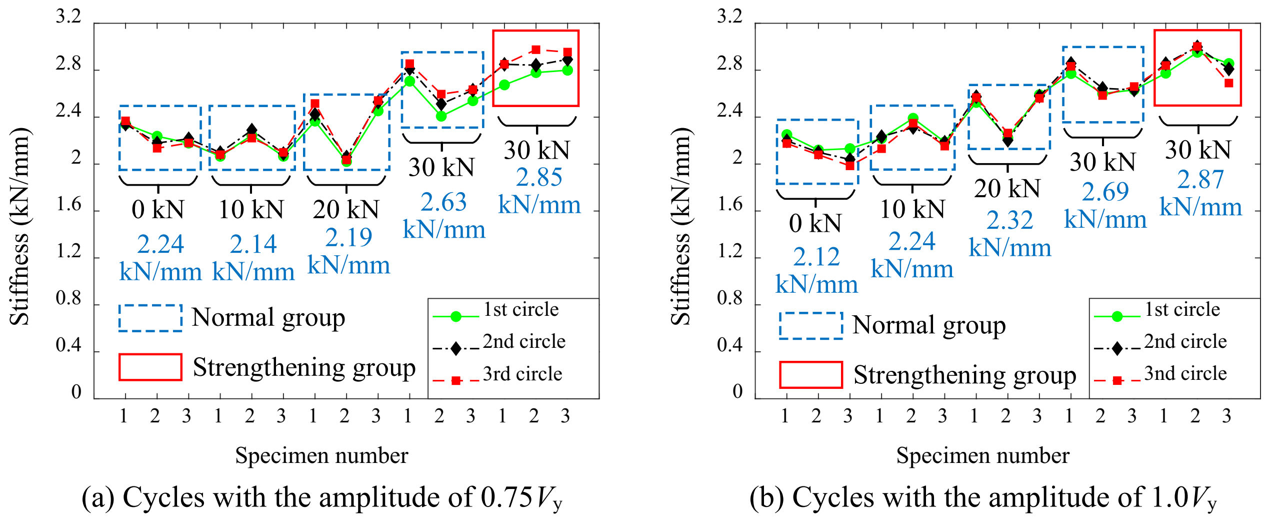

Fig. 13 Scant stiffness of angle brackets under different axial loads

stiffness can be observed. It is because during the cyclic shear tests, a larger co-existent axial tension can allow for a tighter contact between the screws and the surrounding CLT, eliminating the gaps between the screws and the CLT. It would enhance both the bearing due to contact and the friction force between the screws and the surrounding CLT, resulting in a larger hysteretic secant stiffness. Meanwhile, when under the identical axial tension of 30 kN, strengthening the angle brackets using four additional connection-to-floor screws can enhance their secant stiffness by 8.4% and by 6.7% for the cycles with a $0.75V_y$ amplitude and for the cycles with a $1.0V_y$ amplitude, respectively. By increasing the co-existent axial tension, a growing trend of the secant stiffness can be observed for the angle brackets subjected to the cycles with relatively small amplitudes (i.e., $0.75V_y$ and $1.0V_y$). It is because the angle brackets subjected to the cycles with an amplitude of no more than $1.0V_y$ are still within the elastic stage. For the angle brackets with plastic deformation caused by the cycles with an amplitude of $2.0V_y$ or more, increasing the axial tension T could weaken the secant stiffness. For instance, when subjected to cycles with an amplitude of $2V_y$, the average secant stiffness of the angle brackets declined from 1.87 kN/mm to 1.72 kN/mm with an increase of the axial load from 10 to 30 kN. It indicates that a strong tension–shear coupling effect exists in the angle brackets subjected to the cycles with large amplitudes.

Shear strength degradation

The degradation of the shear strength for the cycle i, the D_i was calculated using Eq. (2) to verify the capability of the angle brackets to withstand the cyclic shear force. The angle brackets were approaching to the damages when they were loaded to the cycles with the amplitude of $2V_y$. At this moment, the jack was manually adjusted drastically to maintain a stable co-existent axial tension applied on the specimen. Such an operation could increase the calculation errors of the D_i corresponding to the cycles with an amplitude of $2V_y$. Therefore, for the angle brackets subjected to different levels of co-existent axial tension, the D_i of the second and the third cycles with the amplitude of $0.75V_y$ and that of the second and the third cycles with the amplitude of $1.0V_y$ were calculated, as shown in Fig. 14. Overall, for the cycles with an amplitude of $0.75V_y$ and those with an amplitude of $1.0V_y$, the shear strength degradation is getting worse with an increase of the applied co-existent axial tension. Besides,

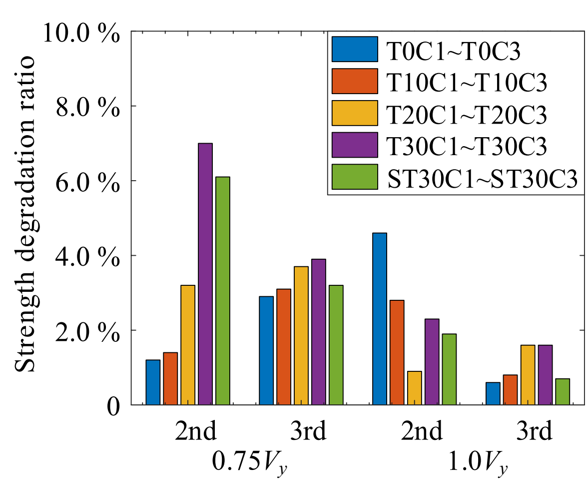

Fig. 14 Shear strength degradation of the angle brackets

when under the identical axial tension of 30 kN, the degradation ratio of the shear strength D_i is compared between the specimens of T30C1–T30C3 and those of ST30C1–ST30C3 (See the purple and the green columns in Fig. 14). It is found that when strengthening the angle bracket using more screws for connecting its horizontal leg to the CLT floor (i.e., from 10 to 14 screws), the D_i can be mitigated by 12.85–56.25%.

$$D_i = 1 - \frac{F_i}{F_{i-1}} \tag{2}$$

Energy dissipation

The energy dissipation from the cyclic shear loading was calculated for the angle brackets in the specimens from both the normal and the strengthening groups. The energy dissipation of the angle brackets in the specimens under both the 0-kN and the 10-kN axial tensions and that of the angle brackets in the specimen under the 30-kN axial tension are shown in Fig. 15a, b, respectively. The energy dissipation of the angle brackets from shear loading enhances when the amplitude of the cycles increases. The energy dissipation increases by 70% approximately when the amplitude increases from $0.75V_y$ to $1.0V_y$. Whereas, when the amplitude further increases from $1.0V_y$ to $2.0V_y$, the energy dissipation increases by almost 4 times. Compared to the energy dissipation for the first cycle with an amplitude of $2.0V_y$, the energy dissipation for the second cycle with an amplitude of $2.0V_y$ reduces significantly (Fig. 15).

For comprehending the influence of the co-existent axial load on the energy dissipation of the angle brackets from the shear loading, the energy dissipations under different levels of axial tension T were compared with respect to each level of the amplitudes (Fig. 16). Applying a co-existent axial tension T on the angle bracket can decrease its energy dissipation from shear loading significantly. For instance, when the amplitude is $0.75V_y$, the average energy dissipation is 0.306 kJ for the axial load of 0 kN. By contrast, for the axial load of 10 kN, the average energy dissipation drops by 65.0% approximately, which is just 0.107 kJ. The energy dissipation of the pair of angle brackets from shear loading is the lowest when the axial tension T increases to 20 kN. When the axial tension T further enhances from 20 to 30 kN, a growing trend of the energy dissipation from shear loading can be observed, which is more pronounced for the amplitude of $2.0V_y$. It indicates that when the angle brackets are subjected to cycles with a larger amplitude, a stronger tension–shear coupling effect can be achieved. For the co-existent axial tension of 30 kN, when strengthening the angle brackets using more connection-to-floor screws, the energy dissipation from shear loading is almost unchanged.

Numerical modeling

Model development

In this study, a detailed numerical model of the specimens was developed based on the commercial software package ABAQUS. It was determined that the model of the specimens in the normal group rather than that of the specimens in the strengthening group was developed based on the following reasons: (1) the specimens in the normal group were tested in shear under four levels of prescribed co-existent axial tension. The shear behavior of the model can be comprehensively validated with

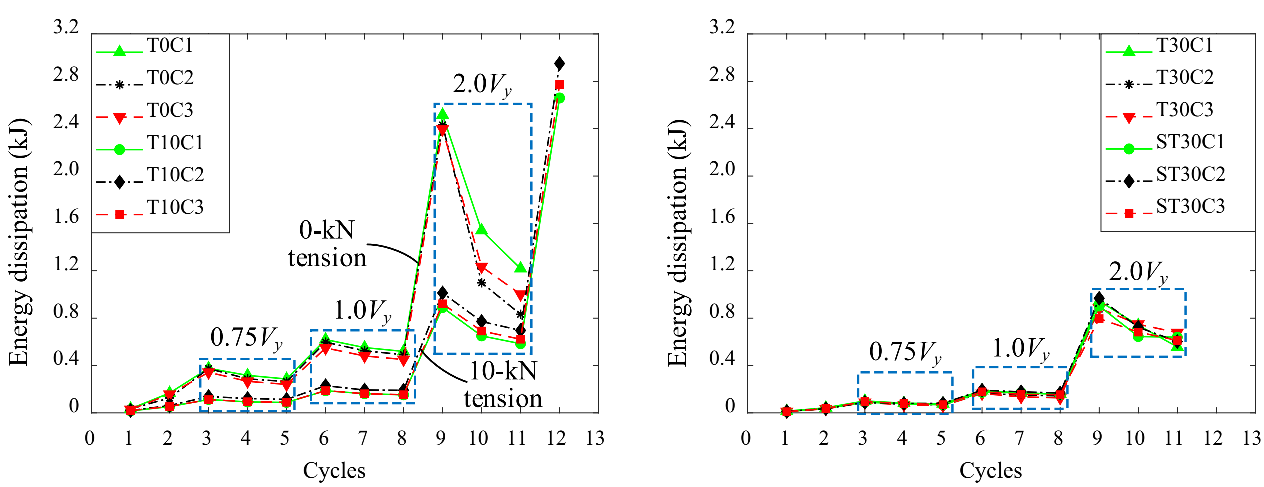

(a) 0-kN and 10-kN axial tensions (b) 30-kN axial tension

Fig. 15 Energy dissipation of the cyclic shear tests

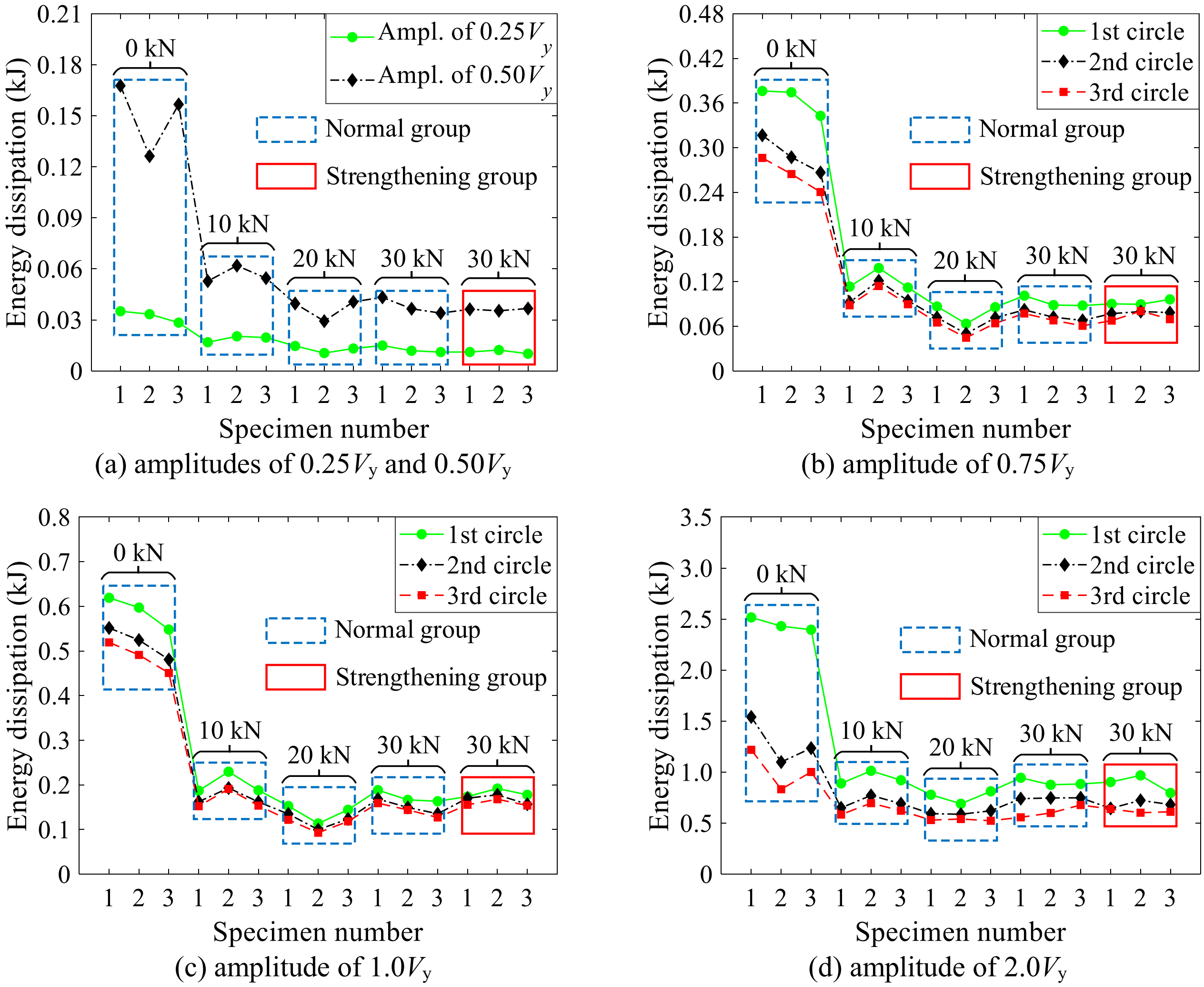

Fig. 16 Influence of axial tension on the energy dissipation from cyclic shear loading

respect to each axial tension level; (2) the $F_{v,max}$ of the specimens could just be enhanced slightly from 48.53 to 51.65 kN, when strengthening the angle brackets using more screws for postponing the preliminary pull-out failure; (3) the premature pull-out failure occurring in the angle brackets of the specimens in the normal group did not weaken their $F_{v,max}$ significantly.

Because a pair of angle brackets was fixed to the CLT wall and the floor diaphragms symmetrically in each specimen, only half of the specimen was considered in the numerical model. It consisted of one 175-mm-thickness CLT floor diaphragm, one 87.5-mm-thickness CLT wall, and one angle bracket. The shear resisting capacity of the specimen should be twice of that calculated from the model. The details of the numerical model of the angle bracket are shown in Fig. 17. Considering that no crushing failure was observed in the CLT after the tests, in the numerical model, a three-dimensional solid

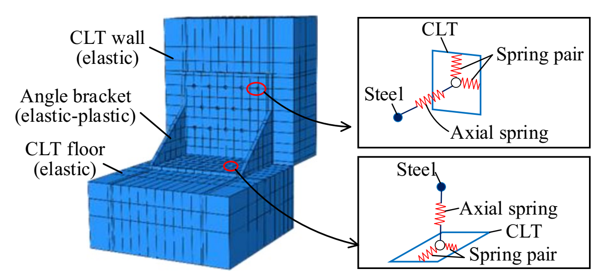

Fig. 17 Numerical model of the angle brackets

element (i.e., type C3D8R in ABAQUS) with an orthotropic elastic material model was used to simulate the CLT. The CLT in-plane elastic modulus along the major strength direction and that along the minor strength direction were defined as 7185 MPa and 4906 MPa, respectively. The CLT out-of-plane elastic modulus was defined as 349 MPa. All the elastic modulus were determined based on the CLT compressive tests conducted by He et al. [2]. An elasto-plastic isotropic material model with a Young's modulus of 210 GPa was assigned to the C3D8R element for simulating the mechanical behavior of the angle brackets. The yielding strength and the Poisson's ratio of the angle brackets were defined as 210 MPa and 0.3, respectively.

One nonlinear oriented spring pair (as ABAQUS user element) with the Q-pinch material model [28] was defined between the angle bracket and the CLT to simulate the shear behavior of the self-tapping screw along both the major strength direction and the minor strength direction of the CLT. The envelope of the Q-pinch material model can be described as an exponential curve with a linear softening segment, which was originally developed by Foschi [29]. For the envelope curve, the relationship between the force F and the displacement δ can be expressed by Eqs. (3)–(5). F_0 is the intercept of the asymptote line; k_1 and k_2 are the initial stiffness of the envelop line and the slope ratio of the asymptote line; F_u and δ_u represent the peak force and the corresponding displacement, respectively; k_3 is the stiffness of the descending segment of the envelop line; δ_F represents the failure displacement. As for the parameters that control the hysteretic behavior of the Q-pinch model, k_4 and k_5 are the unloading stiffness and the stiffness of the pinching segment, respectively. k_6 is the reloading stiffness determined by Eq. (6), in which δ_y is the yielding displacement; δ_{UD} is the unloading displacement; β and α are the stiffness degradation factor and the reloading degradation factor, respectively. It should be noted that the hysteretic rule of the Q-pinch model is different for the small deformation and the large deformation. When within the small deformation, the shear behavior of the nonlinear oriented spring pair with the Q-pinch model follows the hysteretic model developed by Folz and Filiatrault [30] (Fig. 18a). Whereas, when under the large deformation, that shear behavior follows the hysteretic model developed by Stewart [31] for reproducing the pinching effect (Fig. 18b). The parameters of the Q-pinch model assigned to the spring pair can be calibrated based on the results of the cyclic shear tests on the self-tapping screws, which were conducted separately by the authors. The calibrated parameters of the Q-pinch model are listed in Table 4.

$$F(\delta) = \mathrm{sgn}(\delta)\cdot(F_0 + k_2|\delta|)\cdot[1-\exp(-k_1|\delta|/F_0)] \quad (|\delta| \le |\delta_u|) \tag{3}$$

$$F(\delta) = \mathrm{sgn}(\delta)F_u + k_3[\delta - \delta_u\cdot\mathrm{sgn}(\delta)] \quad (|\delta_u| \le |\delta| \le |\delta_F|) \tag{4}$$

$$F(\delta) = 0 \quad (|\delta| \ge |\delta_F|) \tag{5}$$

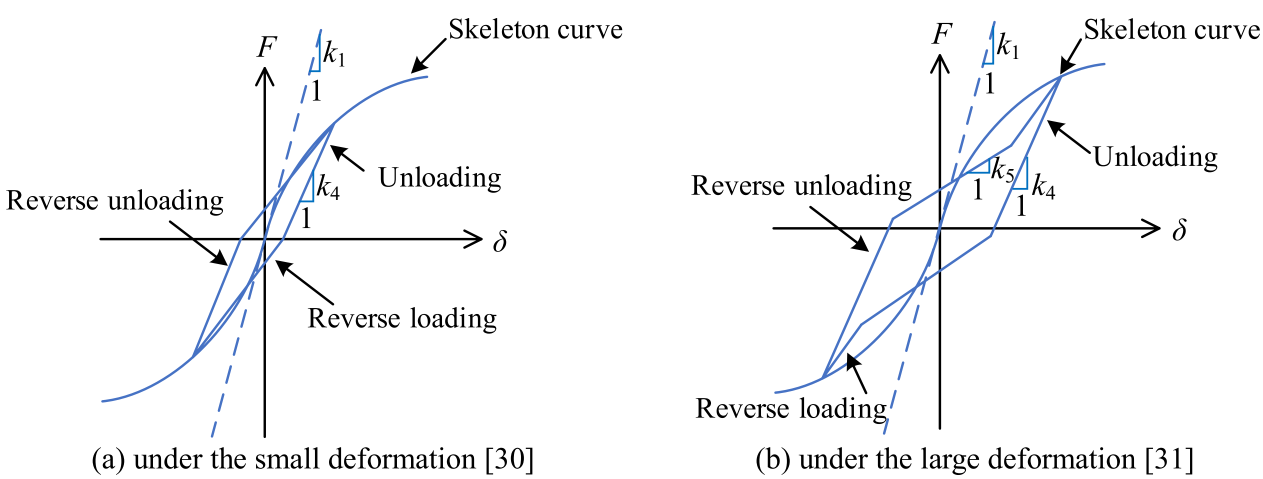

Fig. 18 Hysteretic curve of Q-pinch model

Table 4 Calibrated parameters for the Q-pinch model in the spring pair

Stiffness (N/mm)					Displacement (mm)		Force (N)	Degradation factor	
k_1	k_2	k_3	k_4	k_5	δ_u	δ_F	F_0	α	β
800	244	−170	8200	20	10.21	40	3612	0.8	1.1

Table 5 Calibrated parameters for the Q-pinch model in the axial spring

Stiffness (N/mm)					Displacement (mm)		Force (N)	Degradation factor	
k_1	k_2	k_3	k_4	k_5	δ_u	δ_F	F_0	α	β
4250	220	−150	4250	20	1.45	5.4	4095	0.55	1.1

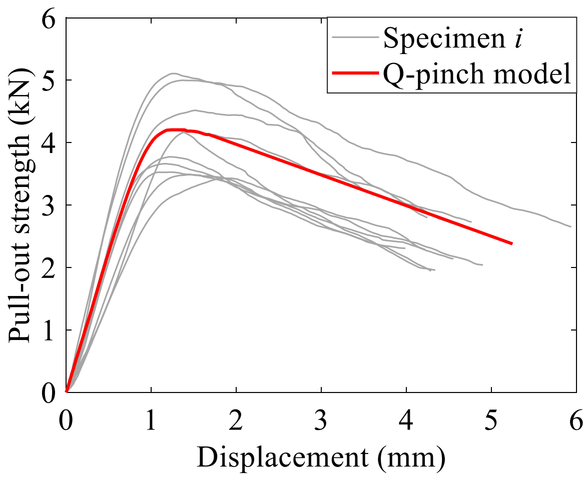

Fig. 19 Comparison between numerical and experimental pull-out curves

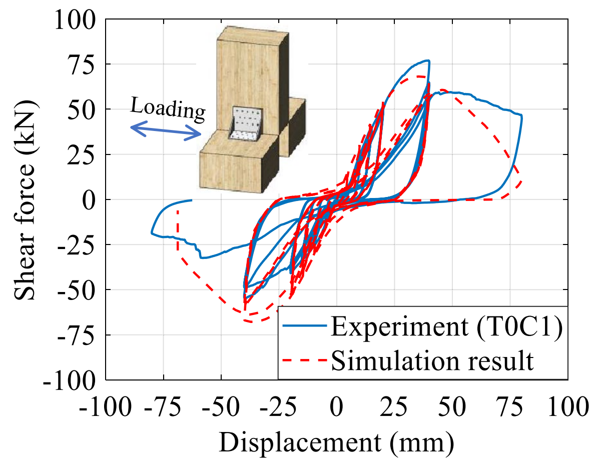

Fig. 20 Comparison of the load–displacement curves under the 0-kN axial load

$$k_6 = k_1 \cdot \left(\frac{\delta_y}{\beta \cdot \delta_{\mathrm{UD}}}\right)^{\alpha} \tag{6}$$

For simulating the pull-out behavior of the self-tapping screws, an axial spring with the Q-pinch material model was defined between the angle bracket and the CLT, the orientation of which was perpendicular to the CLT plane (Fig. 17). Based on the results of the pull-out tests conducted separately on totally 10 self-tapping screws, the parameters for the Q-pinch model in the axial spring were calibrated, as listed in Table 5. Comparison between the numerical curve from the calibrated Q-pinch material model and the experimental curves from the pull-out tests on the screws are shown in Fig. 19. An ideal agreement was achieved, indicating that the axial spring with the Q-pinch material model is capable of reproducing the pull-out behavior of the self-tapping screws drilled into CLT. Besides, the surface-to-surface contact element with a 5.0-kN/mm compressive stiffness was defined between the angle bracket and the CLT wide face. In the contact element, the angle bracket was defined as the master surface, and the CLT panels with a less density and a less-densified mesh was defined as the slave surface. A calibrated coefficient of friction of 0.25 was defined for the contact element to simulate the friction that existed in the contact interface between the angle bracket and the CLT wide face. Both the compressive stiffness of 5.0 kN/mm and the steel-to-CLT friction coefficient of 0.25 were determined based on the studies conducted by Hassanieh et al. [32] and Aira et al. [33].

Model validation

In the ABAQUS software, the explicit dynamic solver was adopted in the iterative calculations of the model. As shown in Fig. 20, when no axial tension is applied, the load–displacement curve of the model from the cyclic shear loading is approximately in agreement with that of the specimen from the cyclic shear test. It should be noted that a little difference can be observed between the numerical cyclic curve and the experimental cyclic curve when the displacement exceeds 40 mm. It is because when the displacement exceeded 40 mm, some damages occurred on the CLT floor panel, which included the localized crushing and the de-lamination failure of the CLT. These damage modes resulted in a significant drop in the shear force measured during the cyclic tests. Whereas, the damage modes of the CLT could not be reflected in the model, otherwise it would bring difficulties in the convergence of the iterative calculations. More efforts will be made in the future to increase the prediction accuracy of the model.

When a constant axial tension T was applied on the specimen, it was difficult to converge for the iterative calculations of the numerical model. This difficulty arose because, during the iterative calculations of the model under a cyclic shear loading, the vertical displacement of the model would simultaneously fluctuate drastically to maintain a constant axial tension, which hindered the convergence of the iterative calculations. Whereas, when under a monotonic shear loading, the model of the specimen with a co-existent axial tension T could provide a numerical monotonic load–displacement curve, which is in agreement with the corresponding load–displacement curve from the monotonic shear test, as shown in Fig. 21. Overall, based on the monotonic loading scenario, the validated model can provide a reliable prediction on the tension–shear coupling effect of the wall-to-floor angle bracket. As for the cyclic loading scenario, more efforts should be conducted in the future to address the convergence of the iterative calculations of the model.

Analytical tension–shear interaction diagram

For obtaining the analytical tension–shear interaction diagram representing the coupling effect of the CLT wall-to-floor angle brackets, comprehensive parametric analysis was conducted to investigate the influence of the co-existent axial tension T on the shear strength of the angle bracket based on the validated numerical model. In the parametric analysis, the axial tension T that was simultaneously applied to the specimen was defined from 0 to 55 kN with a 5-kN interval; besides, one 52-kN axial tension scenario was also considered. The co-existent axial tension T that applied on the specimen should be twice of that applied to the numerical model. Load–displacement curves under monotonic shear loading were obtained from the numerical model and compared for each level of axial tension T applied to the specimen (Fig. 22). The shear

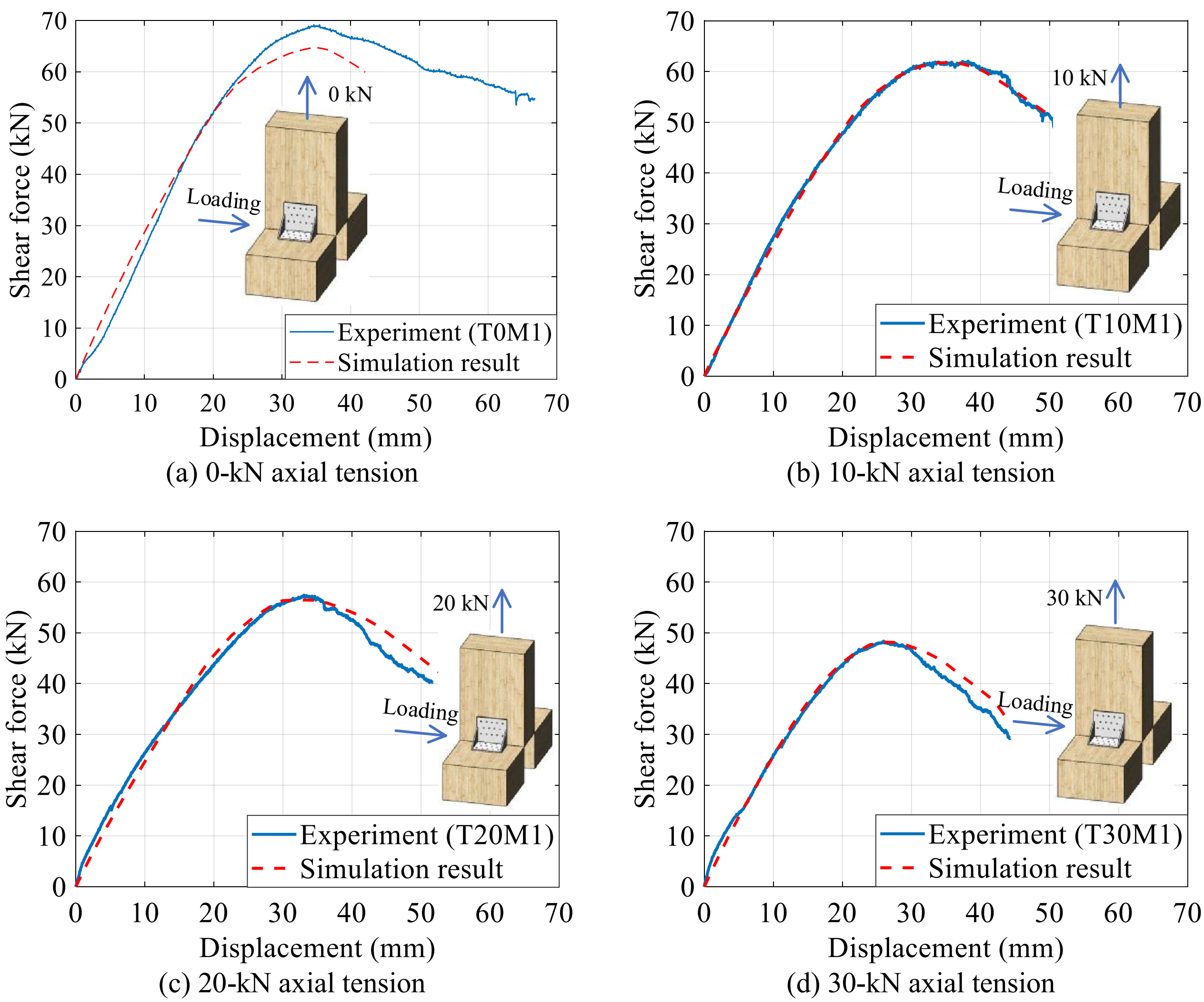

Fig. 21 Experimental curves versus numerical curves

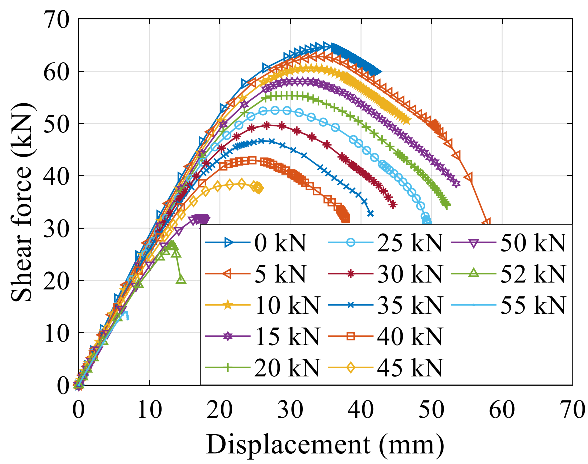

Fig. 22 Monotonic load–displacement curves based on parametric analysis

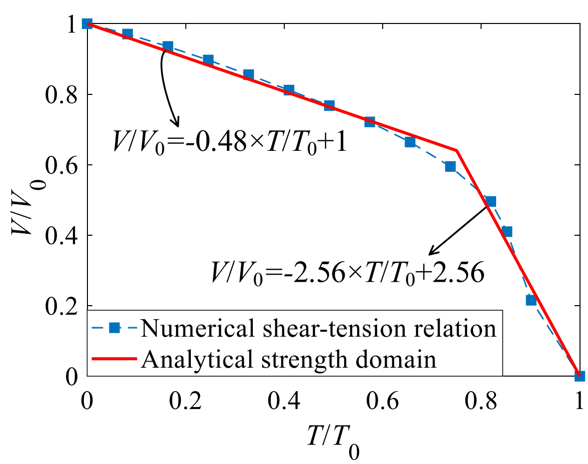

Fig. 23 Numerical tension–shear interaction versus the analytical interaction diagram

resisting capacity V of the specimen under each level of the axial tension T could be obtained based on the monotonic shear-displacement curves in Fig. 21. Furthermore, based on the numerical analysis, when no shear loading was applied, the pull-out resisting capacity T_0 of the specimen was calculated as 61.03 kN. It is noted the T_0 is 6.3% higher than 20 times of the tensile yield strength of the screws (i.e., $20 \times 2.87 = 57.4$ kN). It is because the shear provided by the screws connecting the vertical leg of the angle bracket to the CLT wall also contributed to the T_0. The relationship between the V/V_0 and the T/T_0 is shown in Fig. 23, in which V_0 represents the shear resisting capacity of the specimen when no axial tension was applied, which is 69.15 kN based on the monotonic tests. Based on the regression analysis, an analytical interaction diagram with one bilinear relation between the V/V_0 and the T/T_0 was established approximately, which could represent the tension–shear coupling effect of the angle brackets. The numerical tension–shear interaction relation and the established analytical interaction diagram are compared, as shown in Fig. 23. The analytical interaction diagram can be expressed by Eq. (7).

$$\frac{V}{V_0} = \begin{cases} -0.48\frac{T}{T_0} + 1 & 0 \leq \frac{T}{T_0} \leq 0.75 \\ -2.56\frac{T}{T_0} + 2.56 & 0.75 \leq \frac{T}{T_0} \leq 1 \end{cases} \tag{7}$$

The analytical interaction diagram was derived based on the monotonic action rather than the cyclic action of the angle brackets. The slope of the analytical interaction diagram varied when the T/T_0 reached 0.75, and a bilinear relationship between the V/V_0 and the T/T_0 was established approximately. It is because when the T/T_0 is less than 0.75, i.e., the T applied on the specimen is no more than 45.77 kN, significant plastic deformation due to shear occurred in the self-tapping screws in addition to the connection-to-floor screws being pulled out (See Fig. 4). Especially, when the T is approaching to the 0 kN, the connection-to-floor screws are more prone to a shear-type fracture. By contrast, when the T/T_0 exceeds 0.75, the connection-to-floor screws are pulled out prematurely, so that the shear effect of the screws is hardly exerted. Especially, when the T is approaching to the T_0, the connection-to-floor screws are more prone to a tensile-type fracture. The analytical interaction diagram can be served as a reference for the comprehension of the coupling effect of CLT connections. It should be emphasized that the Eq. (7) is only valid for the angle brackets investigated in the study. For the angle brackets with a different specification, the specific weakening ratio of the force-resisting capacity due to the coupling effect should be determined based on the judgement of the engineers.

Conclusions

In the study, the tension–shear coupling effect under seismic loads was investigated based on monotonic and cyclic shear tests on the CLT wall-to-floor angle brackets, which were simultaneously applied with different levels of co-existent axial tension. The influence of the axial tension on the shear performance of the angle brackets was analyzed, and an analytical interaction diagram representing the coupling effect was obtained. The main findings can be concluded as follows:

1. A larger axial tension can result in a more severe pull-out of the connection-to-floor screws of the

angle brackets after the cyclic shear loading. Besides, when under an identical co-existent axial tension, compared to the monotonic shear loading, the cyclic shear loading can cause a more severe pull-out of the screws.

2. With an increase of the co-existent axial tension from 0 to 30 kN, the shear resistance of the angle brackets is diminished by 33.29%, and the pinching effect of the hysteretic curves is mitigated. When strengthening the angle brackets using more connection-to-floor screws (i.e., from 10 to 14 screws), the shear resistance can be enhanced by 6.43%, and the shear strength degradation is relieved by 12.85–56.25%.
3. When the angle brackets are subjected to the cycles with larger amplitudes, a stronger tension–shear coupling effect can be achieved. When subjected to the cycles with the amplitudes of $0.75V_y$ and $1.0V_y$, the shear strength degradation of the angle brackets is getting worse with an increase of the co-existent axial tension.
4. Applying a co-existent axial tension on the angle brackets can decrease their energy dissipation from shear loading by up to 65.0%. Besides, when strengthening the angle brackets using more connection-to-floor screws, their energy dissipation from the shear loading is almost unchanged.
5. For the CLT wall-to-floor angle brackets, the analytical interaction diagram representing the coupling effect can be expressed by one bilinear function, which consists of the ratio between the shear to the shear resistance and the ratio between the tension to the pull-out resistance.

Acknowledgments
Not applicable.

Author contributions
XS: Data curation, Methodology, Investigation, Software, Writing—review and editing. MH: Conceptualization, Methodology, Investigation. ZL: Conceptualization, Methodology, Investigation.

Funding
The authors gratefully acknowledge the support from National Natural Science Foundation of China (Grant Nos. 52108242 and 52078371), and China Postdoctoral Science Foundation (Grant No. 2021M692444).

Availability of data and materials
The datasets used and/or analyzed during the current study are available from the corresponding author on reasonable request.

Declarations

Ethics approval and consent to participate
Not applicable.

Consent for publication
Not applicable.

Competing interests
There is no competing interests.

Received: 11 April 2023 Accepted: 22 August 2023
Published online: 11 September 2023

References

1. Sun XF, He MJ, Li Z (2020) Novel engineered wood and bamboo composites for structural applications: state-of-art of manufacturing technology and mechanical performance evaluation. Constr Build Mater 249:118751
2. He MJ, Sun XF, Li Z, Feng W (2020) Bending, shear, and compressive properties of three- and five-layer cross-laminated timber fabricated with black spruce. J Wood Sci 66:38
3. Ukyo S, Shindo K, Miyatake A (2019) Evaluation of rolling shear modulus and strength of Japanese cedar cross-laminated timber (CLT) laminae. J Wood Sci 65:31
4. Huang Z, Jiang L, Ni C, Chen ZF (2023) The appropriacy of the analytical models for calculating the shear capacity of cross-laminated timber (CLT) under out-of-plane bending. J Wood Sci 69:14
5. Mohd Yusof N, Md Tahir P, Lee SH, Khan MA, James RMS (2019) Mechanical and physical properties of cross-laminated timber made from Acacia mangium wood as function of adhesive types. J Wood Sci 65:20
6. Bao YW, Lu WD, Yue K, Zhou H, Lu BH, Chen ZT (2020) Structural performance of cross-laminated timber-concrete composite floors with inclined self-tapping screws bearing unidirectional tension–shear loads. J Build Eng 55:104653
7. Gavric I, Fragiacomo M, Ceccotti A (2015) Cyclic behavior of typical metal connectors for cross-laminated (CLT) structures. Mater Struct 48(6):1841–1857
8. Tomasi R, Smith I (2014) Experimental characterization of monotonic and cyclic loading responses of CLT panel-to-foundation angle bracket connections. J Mater Civ Eng 27(6):04014189
9. Hossain A, Danzig I, Tannert T (2016) Cross-laminated timber shear connections with double-angled self-tapping screw assemblies. J Struct Eng 142(11):04016099
10. Izzi M, Flatscher G, Fragiacomo M, Schickhofer G (2016) Experimental investigations and design provisions of steel-to-timber joints with annular-ringed shank nails for cross-laminated timber structures. Constr Build Mater 122:446–457
11. ETA-11/0030 (2016) Screws for use in timber construction. European Technical Assessment, ETA, Denmark
12. Sun XF, He MJ, Li Z, Lam F (2020) Seismic performance of energy-dissipating post-tensioned CLT shear wall structures I: shear wall modeling and design procedure. Soil Dyn Earthq Eng 131:106022
13. Liu JJ, Lam F (2018) Experimental test of coupling effect on CLT angle bracket connections. Eng Struct 171:862–873
14. Liu JJ, Lam F (2019) Experimental test of coupling effect on CLT hold-down connections. Eng Struct 178:586–602
15. Liu JJ, Lam F, Foschi RO, Li MH (2020) Modeling the coupling effect of CLT connections under biaxial loading. J Struct Eng 146(4):04020040
16. Pozza L, Ferracuti B, Massari M, Savoia M (2018) Axial-shear interaction on CLT hold-down connections—experimental investigation. Eng Struct 160:95–110
17. Pozza L, Saetta A, Savoia M, Talledo D (2017) Coupled axial-shear numerical model for CLT connections. Const Build Mater 150:568–582
18. Izzi M, Polastri A, Fragiacomo M (2018) Modeling the mechanical behavior of typical wall-to-floor connection systems for cross-laminated timber structures. Eng Struct 162:270–282
19. D'Arenzo G, Rinaldin G, Fossetti M, Fragiacomo M (2019) An innovative shear–tension angle bracket for cross-laminated timber structures: experimental tests and numerical modeling. Eng Struct 197:109434
20. D'Arenzo G, Casagrande D, Polastri A, Fossetti M, Fragiacomo M, Seim W (2021) CLT shear walls anchored with shear–tension angle brackets: experimental tests and finite-element modeling. J Struct Eng 147(7):04021089

21. Masroor M, Doudak G, Casagrande D (2020) The effect of bi-axial behavior of mechanical anchors on the lateral response of multi-panel CLT shear walls. Eng Struct 224:111202
22. NLGA (2010) Standard grading rules for Canadian lumber. Surrey: National Lumber Grades Authority
23. Sun XF, He MJ, Li Z (2020) Experimental and analytical lateral performance of posttensioned CLT shear walls and conventional CLT shear walls. J Struct Eng 146(6):04020091
24. EN 12512: 2006 (2006) Timber structures—test methods—cyclic testing of joints made with mechanical fasteners. European Committee for Standardization (CEN), Brussels, Belgium
25. Shen YL, Schneider J, Tesfamariam S, Stiemer SF, Mu ZG (2013) Hysteresis behavior of bracket connection in cross-laminated-timber shear walls. Constr Build Mater 48:980–991
26. Pei S, Popovski M, van de Lindt JW (2013) Analytical study on seismic force modification factors for cross-laminated timber buildings. Can J Civ Eng 40:887–896
27. Gavric I, Fragiacomo M, Ceccotti A (2015) Cyclic behavior of typical screwed connections for cross-laminated (CLT) structures. Eur J Wood Wood Prod 73(2):179–191
28. Judd JP (2005) Analytical modeling of wood-frame shear walls and diaphragms. Brigham Young University, Cockermouth
29. Foschi RO (1977) Analysis of wood diaphragms and trusses, part I: diaphragms. Can J Earth Sci 4(3):345–352
30. Folz B, Filiatrault A (2001) Cyclic analysis of wood shear walls. J Struct Eng 127(4):433–441
31. Stewart W (1987) The seismic design of plywood sheathed shear walls. Doctoral thesis, University of Canterbury, Canterbury, New Zealand
32. Hassanieh A, Valipour HR, Bradford MA, Sandhaas C (2017) Modelling of steel–timber composite connections: validation of finite element model and parametric study. Eng Struct 138:35–49
33. Aira JR, Arriaga F, Íñiguez-González G, Crespo J (2014) Static and kinetic friction coefficients of Scots pine (*Pinus sylvestris*), parallel and perpendicular to grain direction. Mater Constr 64(315):e030

Publisher's Note